DOI: 10.1002/ejic.200900626

Ru–Ru Metal–Metal Bonding in the Chains of Edge-Sharing Octahedra of $NdMn_{1.5}Ru_{0.5}O_5$: A Neutron Powder Diffraction and Magnetic Study

Cristina de la Calle,*[a] José A. Alonso,[a] María J. Martínez-Lope,[a] María Retuerto,[a] Mar García-Hernández,[a] and María T. Fernández-Díaz[b]

Keywords: Ruthenium / Metal-metal interactions / Chain structures / Multiferroic oxides / Spin-glass behavior / Neutron diffraction

Four members of a new series of oxides of nominal stoichiometry $NdMn_{2-x}Ru_xO_5$ (x = 0.1, 0.2, 0.4, 0.5) have been prepared in polycrystalline form by wet-chemistry procedures followed by thermal treatment at 1000 °C. $NdMn_{2-x}Ru_xO_5$ materials are isostructural with $NdMn_2O_5$. Their crystal structures have been refined from XRD data and, for the x = 0.5 oxide, from NPD data in the space group *Pbam*. The crystal contains infinite chains of $(Mn,Ru)^{4+}O_6$ octahedra sharing edges, linked together by dimeric $(Mn)^{3+}O_5$ square pyramidal units and NdO_8 polyhedra. There is a slight *anti*-site disordering effect, implying that some Ru cations are introduced at the pyramidal positions. For x = 0.5, the crystallographic formula is $Nd^{3+}(Mn^{4+}_{0.572(4)}Ru^{4+}_{0.428(4)})_{oct}(Mn^{3+}_{0.964(8)}Ru^{3+}_{0.036(8)})_{pyr}O_{4.92(4)}$. The abrupt contraction of the c axis for x = 0.5, together with the short (Mn,Ru)−(Mn,Ru) distances (2.60 Å) observed within the chains of octahedra suggest the presence of Ru–Ru metal bonding for this composition. The magnetic properties are characteristic of spin-glasses, as confirmed by *ac* susceptibility measurements.

Introduction

Complex manganese oxides RMn_2O_5 (R = Y, Bi or rare-earth cations) show a significant magnetoelectric effect.[1–4] The interplay between ferroelectricity and magnetism in the RMn_2O_5 oxides suggests the appealing possibility of controlling the polarisation by the application of an external magnetic field which would allow the design of new devices for practical applications. A serious drawback of these phases is the relatively low temperature at which this phenomenon occurs. The temperature of the ferroelectric transitions in the RMn_2O_5 compounds is rather low (30–40 K)[5–7] and the realisation of the magnetoelectric effect in these systems at higher temperatures remains a challenging problem. Therefore, the search for new compounds susceptible to show similar effects at higher temperatures is certainly attractive.

All the RMn_2O_5 (R = La, Pr, Nd, Sm, Eu, Tb, Ho, Er) oxides are isostructural (space group *Pbam*, Z = 4) and contain two crystallographic sites for Mn atoms with different oxygen coordination and oxidation states.[8–10] The structure contains infinite chains of $Mn^{4+}O_6$ octahedra sharing edges, linked together by $Mn^{3+}O_5$ and RO_8 units. Mn^{4+} ions are located at the 4*f* sites, octahedrally coordinated to oxygen atoms, whereas Mn^{3+} ions occupy the 4*h* sites and they are bonded to five oxygen atoms, forming a distorted tetragonal pyramid.

With the aim of inducing new magnetic interactions in the members of the RMn_2O_5 family, we designed and prepared $RFeMnO_5$ (R = Y, Ho, Er),[11–13] $RCrMnO_5$ (R = Y, Dy)[14,15] and $YGaMnO_5$[16] oxides which are obtained by replacing Mn^{3+} by Fe^{3+}, Cr^{3+} and Ga^{3+}, respectively. The introduction of Fe leads to important modifications in the magnetic behaviour. $RFeMnO_5$ display a ferrimagnetic magnetic structure below $T_C \approx 165$ K (R = Y, Er) or 153 K (R = Ho). The magnetic moments of the Mn^{4+} and Fe^{3+} cations are antiferromagnetically coupled, lying along the c direction.[11–13] When Cr is introduced, an important level of cationic disorder was found between both metallic sites (Mn and Cr). Although the magnetic susceptibility indicates the onset of magnetic ordering below $T_C \approx 85$ K, low-temperature NPD patterns do not exhibit any additional magnetic contribution, confirming that long-range magnetic ordering is not fully established.[14,15] Finally, the presence of nonmagnetic Ga at the square pyramidal positions dramatically simplifies the magnetic interactions in this structural type, allowing the manifestation of ferromagnetic interactions along the chains of MnO_6 octahedra which in the parent compound YMn_2O_5 are overcome by strong antiferromagnetic Mn^{4+}–O–Mn^{3+} interactions between the octahedra and the pyramidal units giving rise to an overall incommensurate magnetic structure along the c axis.[16]

In this paper we report on the preparation of the novel series of $NdMn_{2-x}Ru_xO_5$ ($0 \leq x \leq 0.5$) materials which are

[a] Instituto de Ciencia de Materiales de Madrid, CSIC, Cantoblanco, 28049 Madrid, Spain
E-mail: c.delacalle@icmm.csic.es
[b] Institute Laue-Langevin (ILL) 156X, 38042 Grenoble Cedex 9, France

isostructural with the RMn_2O_5 compounds and are obtained by substitution of Ru by Mn cations. Our aim was to enhance the effects observed in the Fe-doped series, given the larger spatial extension of the 4d Ru orbitals. These new compounds have been synthesised by a soft-chemistry procedure followed by annealing in air and they have been structurally characterised from XRD and NPD data. This study is complete with macroscopic magnetic susceptibility measurements.

Results

Synthesis

$NdMn_{2-x}Ru_xO_5$ ($0 < x \leq 0.5$) have been obtained by thermal treatment in air and at ambient pressure. For x = 0.1, 0.2 and 0.4, they are perfectly pure phases. For the product with x = 0.5, a quantity of about 3% of $NdMnO_3$ perovskite remained present as indicated by XRD and NPD analysis. Attempts to synthesise with Yttrium (Y) and other rare earths (La, Tb, Dy, Ho, Er, Tm, Yb and Lu) instead of Nd did not yield the RMn_2O_5 crystal structure. With Y and the small-sized cations of the rare earths (Tb, Dy, Ho, Er, Tm, Yb and Lu) a segregation of RuO_2 and the pyrochlore-like $R_2Mn_{2-x}Ru_xO_7$ phases was observed. For R = La, a majority $LaMnO_3$ perovskite-like phase (perhaps partially Ru-doped) is stabilised.

Crystal Structures

The XRD patterns of the $NdMn_{2-x}Ru_xO_5$ ($0 < x \leq 0.5$) compounds show well defined reflections corresponding to orthorhombic unit cells, isostructural with RMn_2O_5, as displayed in Figure 1. Table 1 lists the unit cell parameters and volume for $NdMn_{2-x}Ru_xO_5$ ($0 \leq x \leq 0.5$) determined from XRD data at room temperature and Figure 2 shows the evolution of the unit cell parameters as a function of the value of x. There is an initial expansion of the unit cell parameters given the larger ionic size of Ru cations. It is noteworthy that the c parameter suddenly decreases for x = 0.5, indicating a contraction of the chains of octahedra (this will be discussed later on). The structures were defined in the orthorhombic space group *Pbam* (No. 55). Nd atoms are located at 4 *g* positions, (Mn,Ru)1 atoms at 4*f*, (Mn,Ru)2 atoms at 4*h* and the four crystallographically independent oxygen atoms at 4*e*, 4 *g*, 4*h* and 8*i* positions. A good fit between the observed and the calculated profiles was obtained after the Rietveld refinement of the crystal structures, as illustrated in Figure 3.

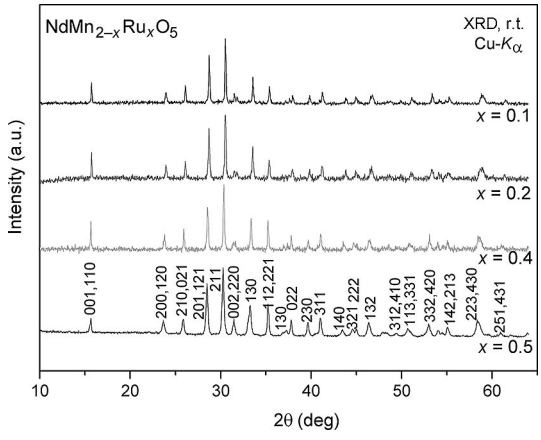

Figure 1. XRD patterns of $NdMn_{2-x}Ru_xO_5$. The x = 0.5 pattern is indexed in an orthorhombic unit cell. Space group *Pbam*.

Table 1. Unit-cell parameters and volume for $NdMn_{2-x}Ru_xO_5$ determined from XRD data at room temperature.

x	a [Å]	b [Å]	c [Å]	V [Å^3]
0.0[a]	7.5051(2)	8.6209(2)	5.7022(1)	368.93(3)
0.1	7.5093(8)	8.6321(8)	5.7166(6)	370.5(1)
0.2	7.521(1)	8.647(1)	5.727(1)	372.5(1)
0.4	7.549(1)	8.675(1)	5.7302(9)	375.2(1)
0.5	7.566(1)	8.691(1)	5.7153(7)	375.8(1)

[a] Taken from ref.[10]

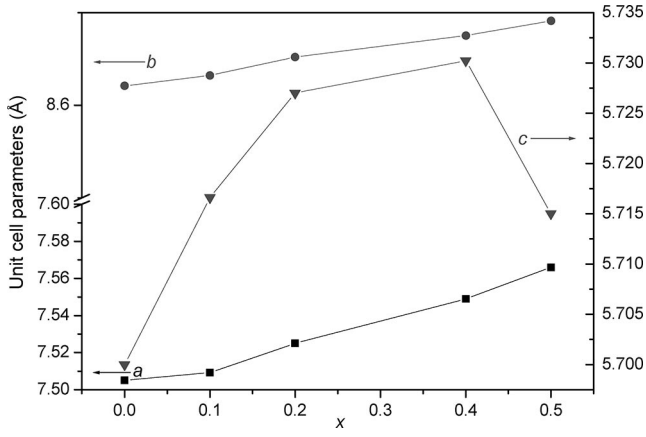

Figure 2. Unit cell parameter variation for $NdMn_{2-x}Ru_xO_5$.

In spite of the minor $NdMnO_3$ impurity present in the sample with x = 0.5, this material was selected for performing a structural NPD study in order to probe the effect of the Ru introduction into the $NdMn_2O_5$ crystal structure since it contains the maximum possible amount of Ru. Ru atoms were initially considered to be distributed at random at the 4*f* (octahedral) sites and then the possibility of *anti*-site disordering (Ru at 4*h* sites) was also explored. The Mn/Ru occupancy factors were independently refined in both sites which resulted in a slight departure from the initial stoichiometry (Mn/Ru = 1.5:0.5). At the octahedral positions, 43% of Mn 4*f* positions are occupied by Ru cations (Ru^{4+}) whereas 4% of Mn 4*h* positions (pyramidal sites) are occupied by Ru cations (probably Ru^{3+}) as shown in Table 2. The occupancy factors of oxygens were also refined; O3 is slightly deficient while the others oxygen atoms are stoichiometric. The refined structural formula is:

$$Nd^{3+}(Mn^{4+}_{0.572(4)}Ru^{4+}_{0.428(4)})_{oct}(Mn^{3+}_{0.964(8)}Ru^{3+}_{0.036(8)})_{pyr}O_{4.92(4)}.$$

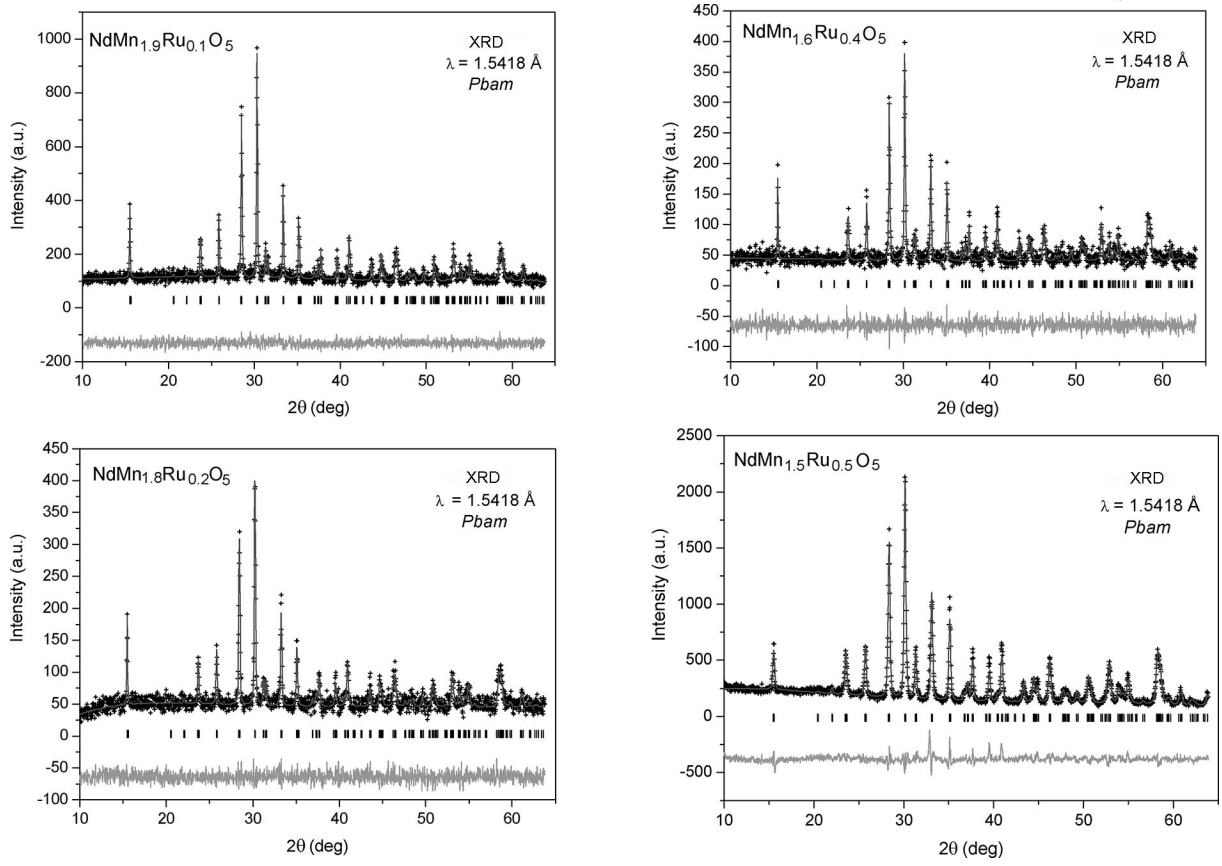

Figure 3. Rietveld plots for $NdMn_{2-x}Ru_xO_5$ from XRD data.

Table 2. Atomic coordinates and isotropic displacement factors for $NdMn_{1.5}Ru_{0.5}O_5$ from NPD data at 295 K. Space group *Pbam*, Z = 4. The z parameters for Mn1 and Ru1 are taken from the XRD refinement.

Atom	Site	x	y	z	B [Å^2]	f_{occ}
Nd	4 *g*	0.1441(6)	0.1721(5)	0.0	0.44(9)	1.0
Mn1	4*f*	0.0	0.5	0.2726(14)	0.3	0.572(4)
Ru1	4*f*	0.0	0.5	0.2726(14)	0.3	0.428(4)
Mn2	4*h*	0.4142(12)	0.3542(9)	0.5	0.2(2)	0.964(8)
Ru2	4*h*	0.4142(12)	0.3542(9)	0.5	0.2(2)	0.036(8)
O1	4*e*	0.0	0.0	0.2708(14)	1.1(1)	1.0
O2	4 *g*	0.1601(9)	0.4492(6)	0.0	0.3(1)	1.0
O3	4*h*	0.1590(11)	0.4342(6)	0.5	0.4(2)	0.92(2)
O4	8*i*	0.4005(4)	0.2099(4)	0.2513(8)	0.27(8)	1.0

Discrepancy factors: R_p = 4.45%, R_{wp} = 5.63%, R_{exp} = 3.99%, χ^2 = 1.99, R_{Bragg} = 7.28%.

It is worth underlining that the refinement of the mixed occupancy factors of Ru and Mn over the same crystallographic site is very precise by neutron diffraction given the opposite values of the scattering lengths for Ru (7.030 fm) and Mn (–3.730 fm). For the same reason, and given the Ru/Mn ratio found at the 4*f* positions, the average scattering length of this site is rather weak and the error in the determination of the corresponding atomic parameters and displacement factor is huge. As a consequence, in the final refinement, the positions for the *4f* sites were fixed to those determined by X-ray diffraction and the displacement factor was set to 0.3 Å^2.

Table 2 lists the structural parameters together with the unit-cell parameters refined from NPD at room temp. for the compound with x = 0.5. Figure 4 (a) shows a good fitting between calculated and observed profiles − the second series of Bragg position markers corresponds to $NdMnO_3$. Table 3 includes the mean interatomic distances and Table 4 gives some selected bond angles for this phase at room temp.

A view of the crystallographic structure approximately along the c axis is displayed in Figure 5. There are two different oxygen environments for the cations that occupy the 4*f* and 4*h* sites. At the 4*f* site, the (Ru^{4+}, Mn^{4+}) cations

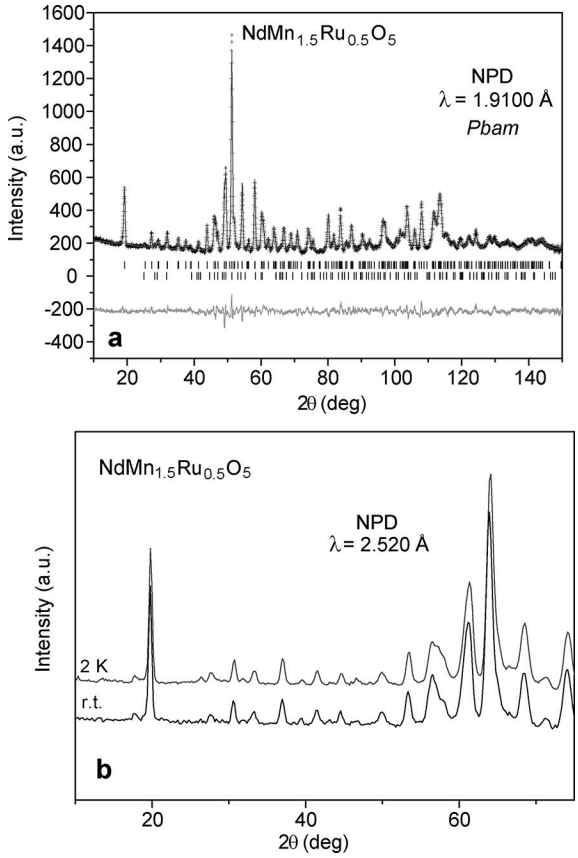

Figure 4. (a) Observed (crosses), calculated (solid line) and difference (bottom line) NPD patterns at room temperature for $NdMn_{1.5}Ru_{0.5}O_5$ (D1A data). The second series of Bragg positions corresponds to the minor impurity $NdMnO_3$. (b) Comparison of observed NPD data at room temperature and at low temperature (D1B data).

Table 3. Selected interatomic distances [Å] for x = 0.5 at room temp. from NPD data.

NdO_8 bicapped prism		
Nd–O1	(×2)	2.415(6)
Nd–O2		2.412(7)
Nd–O2		2.440(7)
Nd–O4	(×2)	2.439(5)
Nd–O4	(×2)	2.554(5)
<Nd–O>		2.458
$(Mn,Ru)1O_6$ octahedron		
(Mn,Ru)1–O2	(×2)	2.025(4)
(Mn,Ru)1–O3	(×2)	1.863(6)
(Mn,Ru)1–O4	(×2)	1.978(3)
<(Mn–Ru)1–O>		1.955
$Mn2O_5$ tetragonal pyramid		
Mn2–O1	(×2)	1.936(9)
Mn2–O3		2.054(12)
Mn2–O4	(×2)	1.900(7)
<Mn–O>		1.945
Mn–Ru distances		
(Mn,Ru)1–(Mn,Ru)1		2.6026(4)
(Mn,Ru)1–(Mn,Ru)1		3.1199(1)
Mn2–Mn2		2.849(12)

(M^{4+}) are inside the $M^{4+}O_6$ distorted octahedra whereas at the 4*h* site, the Mn^{3+} ions form $Mn^{3+}O_5$ distorted tetragonal pyramids (containing just 4% of Ru atoms). The $M^{4+}O_6$ octahedra share edges via O2 and O3 in infinite chains along the *c* axis. The pyramids share edges to form dimeric Mn_2O_5 units linked through two O1 oxygens. The different chains of octahedra are interconnected through the pyramidal dimer units via O3 and O4.

Table 4. Selected bond angles [°]. M1 stands for (Mn,Ru)1.

O2–M1–O2	79.2(4)
O2–M1–O3	94.8(2), 172.9(5)
O2–M1–O4	85.7(3), 88.8(3)
O3–M1–O3	91.4(6)
O3–M1–O4	94.6(4), 90.3(4)
O4–M1–O4	172.9(4)
O1–Mn2–O1	85.3(6)
O1–Mn2–O3	95.4(6)
O1–Mn2–O4	86.4(4)
O3–Mn2–O4	99.9(5)
O4–Mn2–O4	97.0(4)
Mn2–O1–Mn2	94.7(7)
M1–O2–M1	100.8(2)
M1–O3–M1	88.6(2)
M1–O3–Mn2	135.4(6)
M1–O4–Mn2	122.8(5)

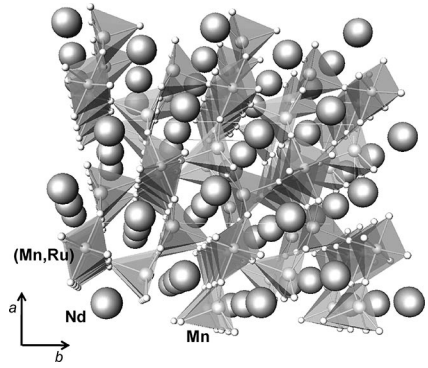

Figure 5. A view of the crystallographic structure of $NdMn_{1.5}Ru_{0.5}O_5$, approximately along the *c* axis. Octahedra and tetragonal pyramids correspond to $(Mn,Ru)^{4+}O_6$ and $(Mn)^{3+}O_5$ polyhedra. The octahedra share edges, forming infinite chains along the *c* axis. The pyramids form dimeric units linking together the chains of octahedra. The spheres represent the Nd atoms.

The low temperature NPD patterns of $NdMn_{1.5}Ru0_{0.5}O_5$ do not show any additional reflections that could suggest the presence of long-range magnetic ordering, as illustrated in part b of Figure 4 in which the patterns collected at room temp. and 2 K in the D1B diffractometer are compared.

Magnetic Measurements

The *dc* susceptibility vs. temperature data for the phases with x = 0.1, 0.2 and 0.5 are shown in Figures 6 and 7. The curves are very similar to those exhibited by the parent compound, $NdMn_2O_5$.[10] A cusp in the FC susceptibility curve suggests antiferromagnetic behaviour at low temperatures. In $NdMn_2O_5$, this maximum (at 5 K) is related to the transition to a modulated magnetic structure. In the present case, the maxima are observed at higher temperatures as listed in Table 5. The insets of Figures 6 and 7 show more

details of the ZFC and FC curves for the samples with x = 0.1, 0.2 and 0.5. Both curves overlap at high temperatures but diverge on decreasing the temperature below ca. 40 K. The antiferromagnetic Néel temperatures can be obtained from the maxima of the ZFC curves listed in Table 5. The splitting of the ZFC and FC curves suggests the presence of an irreversibility and is symptomatic of spin-glass-like behaviour.

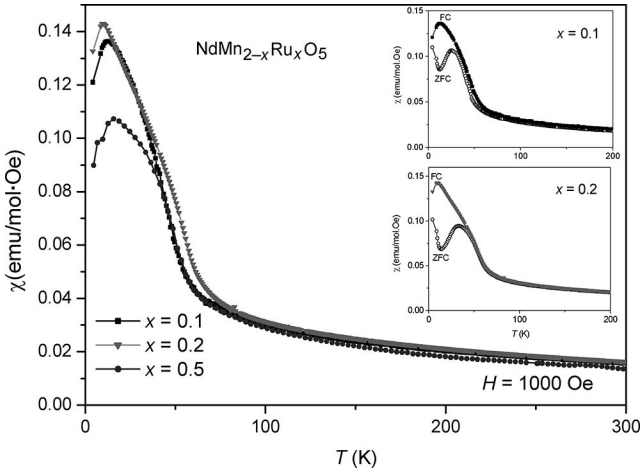

Figure 6. Thermal evolution of the FC magnetic susceptibility measured in a 1 kOe magnetic field for $NdMn_{2-x}Ru_xO_5$. The insets detail the ZFC and FC evolution for x = 0.1 and x = 0.2.

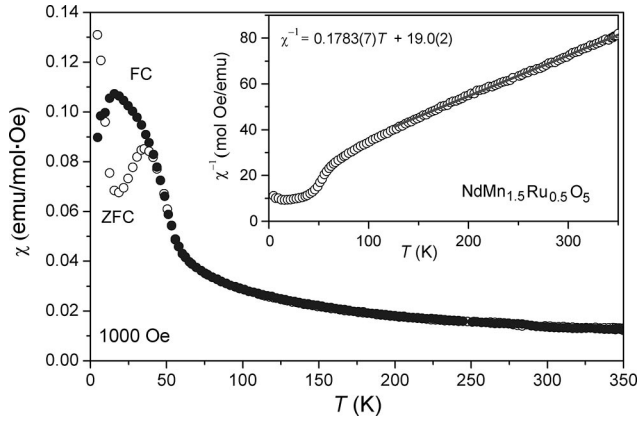

Figure 7. ZFC and FC *dc* susceptibility for x = 0.5. The inset corresponds to the reciprocal susceptibility and the Curie–Weiss fit.

Table 5. Magnetic parameters for $NdMn_{1-x}Ru_xO_5$, from magnetic susceptibility data. The Curie constant C is given in emu mol^{-1} Oe^{-1} K. The T_N was obtained from the maxima of the ZFC curve.

x	Max_{ZFC} [K]	T_N [K]	C	θ_{Weiss} [K]	μ_{eff} [μ_B/f.u.]	μ_{calc}
0.1	12.7	26.0	7.68(1)	–146.2(6)	7.87(1)	7.16
0.2	9.6	33.2	7.51(3)	–128.5(1)	7.51(3)	7.11
0.5	15.7	40.0	5.61(2)	–106.63(2)	6.68(2)	6.94

The paramagnetic regime has been studied from the reciprocal susceptibility plots, illustrated in the inset of Figure 7 for x = 0.5. In the temperature interval 120 K < T < 350 K, the reciprocal susceptibility increases linearly, revealing paramagnetic behaviour. A linear Curie–Weiss fit in this region gives a Curie constant of C = 5.61(2) emu mol^{-1} Oe^{-1} K, a Weiss constant of θ_{Weiss} = –106.63(2) K (the negative Weiss constant is an indicative of antiferromagnetic interactions in this compound) and an effective moment of μ_{eff} = 6.68(2) μ_B/f.u. (6.85 μ_B/f.u. for the parent compound $NdMn_2O_5$). For the x = 0.1 and 0.2 compounds, the corresponding magnetic parameters are included in Table 5. An estimation of the theoretical effective magnetic moment can be gained by considering the expression $\mu_{eff} = [n_{Nd3+}(\mu_{Nd3+})^2 + n_{Mn4+}(\mu_{Mn4+})^2 + n_{Mn3+}(\mu_{Mn3+})^2 + n_{Ru4+}(\mu_{Ru4+})^2 + n_{Ru3+}(\mu_{Ru3+})^2]^{1/2}$. For x = 0.5, n_{Nd3+} = 1.0, n_{Mn4+} = 0.572; n_{Mn3+} = 0.964, n_{Ru4+} = 0.428 and n_{Ru3+} = 0.036 (the n values were determined by the neutron diffraction study). We suppose that the Mn cations are in a high spin (HS) state and Ru cations in a low spin (LS) state and, therefore, μ_{Nd3+} = 3.6 μ_B, μ_{Mn4+} = 3.87 μ_B, μ_{Mn3+} = 4.90 μ_B, μ_{Ru4+} = 2.83 μ_B and μ_{Ru3+} = 1.73 μ_B. The experimental result for the effective magnetic moment is in reasonable agreement with the expected moment of 6.94 μ_B/f.u. For x = 0.1 and 0.2, the expected paramagnetic moments included in Table 5 have been estimated from the nominal stoichiometric coefficients, assuming that Ru^{4+} occupies the octahedral 4*f* sites.

The magnetization isotherms at 4 K (Figure 8) show the almost linear behaviour characteristic of antiferromagnets. There is only a very small curvature and a narrow hysteresis cycle at very low applied magnetic fields for x = 0.5 as illustrated in the inset of Figure 8. This suggests a weak ferromagnetism effect or subtle canting of the magnetic moments.

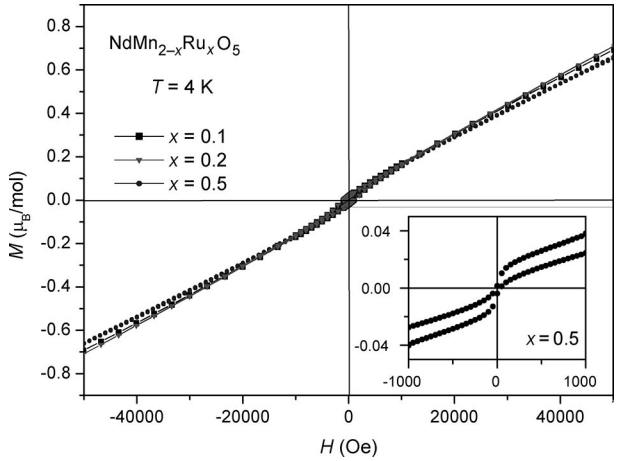

Figure 8. Isothermal magnetisation curves for $NdMn_{2-x}Ru_xO_5$. The inset shows the narrow hysteresis cycle for x = 0.5 between –1000 and 1000 Oe.

The glassy behaviour suggested by the divergence of the FC and ZFC curves has been investigated in detail by *ac* susceptibility for x = 0.5. The thermal evolution of the *ac* susceptibility is shown in Figure 9 for temperatures ranging

from 2 K to 100 K at different frequencies (f) varying from 1 to 10 kHz. χ' and χ'' represent, respectively, the real (in phase) and imaginary (out of phase) components of the susceptibility. Both χ' and χ'' show a sharp increase below 60 K with a maximum at about 48 K; this temperature corresponds to the onset of long-range magnetic interactions, slightly below the magnetic ordering temperature determined by the *dc* susceptibility measurements (T_N = 40 K, in Table 5). There is another peak at lower temperature with a maximum at around 8–9 K. This second anomaly of the χ' curve is slightly frequency dependent. The signal of the imaginary part of the curve is very weak and falls inside the detection limit of the equipment so it is difficult to draw conclusions from the frequency dependence of this part of the *ac* susceptibility.

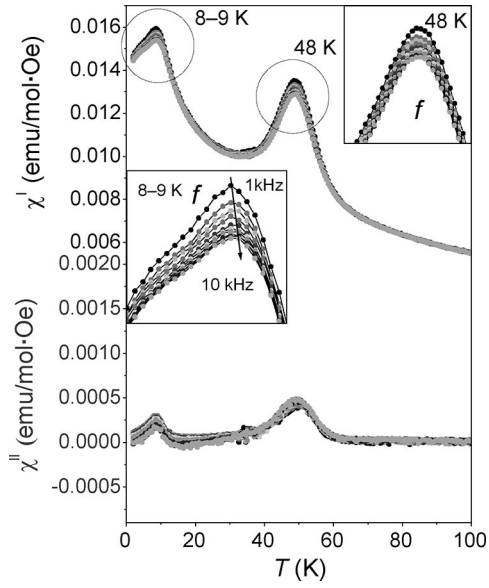

Figure 9. Real and complex *ac* magnetic susceptibilities for $NdMn_{1.5}Ru_{0.5}O_5$. The insets show the frequency dependence of the maxima for the real component. The frequency varies from 1 kHz (top) to 10 kHz (bottom).

Discussion

The products with nominal stoichiometry $NdMn_{2-x}Ru_xO_5$ derive from the parent $NdMn_2O_5$ oxide (containing one Mn^{3+} and one Mn^{4+} cation per formula) by partial replacement of Mn by Ru cations. The structures of the phases with $0 < x \leq 0.5$ were refined from XRD data in the orthorhombic space group *Pbam* (No. 55) and found to be isostructural to $NdMn_2O_5$.[10] Details of the structural modification upon Ru doping were investigated from NPD data in a sample of nominal composition $NdMn_{1.5}Ru_{0.5}O_5$, taking advantage of the large contrast existing between the scattering lengths of Ru and Mn. The first conclusion of this study is that Ru cations preferentially occupy the 4*f* octahedral positions randomly distributed with Mn^{4+} ions. Only 4% of the pyramidal positions at 4*h* are occupied by Ru (probably Ru^{3+}) cations. This is in contrast with that found in the Fe-substituted series $RFeMnO_5$[11–13] where Fe^{3+} preferentially occupies the pyramidal positions. This fact is probably a consequence of the propensity of Ru for adopting a tetravalent oxidation state under the synthesis conditions in air thus favouring its incorporation at the octahedral positions together with Mn^{4+} whereas, in the Fe-substituted series, Fe^{3+} is stabilised with an ionic size suitable for occupying the square-planar pyramidal sites. However, in the case of the chromium-substituted series $RCrMnO_5$,[14,15] the relative easiness of oxidation of Cr to the tetravalent state under moderate oxygen pressure accounts for its incorporation at both octahedral and pyramidal positions, giving rise to an extraordinary *anti*-site effect.

It is interesting to compare the crystal structures of $NdMn_{1.5}Ru_{0.5}O_5$ and $NdMn_2O_5$. For $NdMn_{1.5}Ru_{0.5}O_5$ the volume of the orthorhombic unit cell is larger than for $NdMn_2O_5$, of 368.93 Å,[10] as expected from the difference in ionic radii between Ru^{4+} (0.62 Å) and Mn^{4+} (0.53 Å) in sixfold coordination. In $NdMn_2O_5$ (and other RMn_2O_5 compounds) the $Mn^{4+}O_6$ octahedra are fairly flattened with two bonds significantly shorter than the remaining four bonds, e.g. the Mn–O3 bond length is 1.870(5) Å and the average Mn1–O distance is 1.914 Å.[10] This is also observed in $NdMn_{1.5}Ru_{0.5}O_5$ with (Mn,Ru)1–O3 distances of 1.863(6) Å and an average value of 1.955 Å. Very interestingly, the substitution of Ru^{4+} by Mn^{4+} leads to an unequal variation in the (Mn,Ru)1–(Mn,Ru)1 distances compared with the Mn–Mn in-chain distance in $NdMn_2O_5$ in such a way that there are pairs or dimers of metals at extremely short distances of 2.6026(4) Å. This suggests the existence of metal–metal bonding along the chains of octahedra, probably occurring between pairs of Ru–Ru cations randomly distributed along the chains. For the compound with x = 0.5, the Mn^{4+}/Ru^{4+} ratio is approximately unity which would optimise this interaction even if Mn and Ru are totally disordered in the crystal. No superstructure peaks have been observed either in the XRD or NPD patterns which could indicate the presence of long-range Ru–Mn ordering. However, the abrupt shrinkage of the *c* unit-cell parameter is also indicative of the establishment of Ru–Ru direct bonds for this particular x = 0.5 composition. The mentioned short distance is comparable to that existing in other compounds presenting Ru–Ru bonding such as the hexagonal 9R-$BaRuO_3$ polytype of perovskite (2.55 Å).[17] In this example, the chains of RuO_6 octahedra share faces along the *c* axis whereas in the present case the $(Mn,Ru)O_6$ octahedra share edges along *c*. Instead of a random distribution of Mn and Ru atoms, we can think of a random distribution of Ru–Ru couples along *c* leading to the formation of Ru–Ru bonding wherever the Ru–Ru couples spontaneously occur as shown in Figure 10. The observed (Mn,Ru)-1−(Mn,Ru)1 distance of 2.6026(4) Å indeed corresponds to the average distance between Mn–Mn and Ru–Ru pairs, so it is reasonable to think that the local Ru–Ru bond lengths are even shorter. For the compound with x <0.5 which shows a much larger *c* parameter, the occurrence of direct Ru–Ru bonds is presumably less pronounced given the dilution of Ru^{4+} cations in the Mn^{4+} chains. This is the first

time, to the best of our knowledge, that metal–metal bonding has been identified within the chains of edge-sharing octahedra in this structural type.

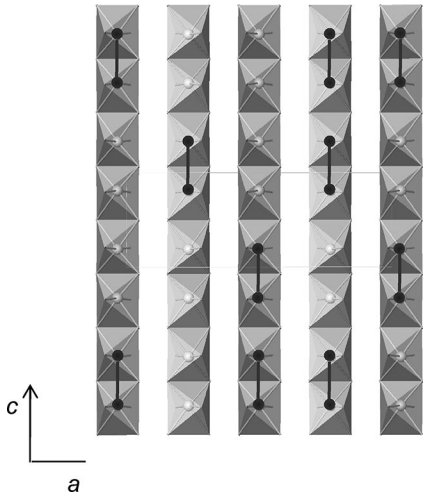

Figure 10. Schematic representation of the random distribution of Ru–Ru pairs (dark bonded atoms) along the chains of $(Mn,Ru)O_6$ octahedra.

Regarding the tetragonal pyramids occupied mostly by Mn^{3+}, containing only 4% of Ru, we believe that Ru^{3+} would be more suitable for occupying this site. Since there are no tabulated data for fivefold coordination, we can compare the ionic sizes of Ru^{3+} (0.68 Å) with HS-Mn^{3+} (0.645 Å) in sixfold coordination.[18] The pyramidal $Mn^{3+}O_5$ units are elongated since the axial Mn2–O3 bond length is the largest [2.054(12) Å], although this effect is less pronounced than in $NdMn_2O_5$ [2.076(7) Å], given the small content of non-Jahn–Teller Ru^{3+} cations. With respect to the oxygen coordination of Nd^{3+} cations, it can be described as $Nd^{3+}O_8$ bicapped prisms, with average <Nd–O> distances of 2.458 Å which is in good agreement with the average <Nd–O> bonds lengths of 2.451 Å observed in $NdMn_2O_5$.[10]

The *dc* susceptibility measurements indicate a long-range magnetic order with cusps in the FC susceptibility curves in the 9–16 K range, suggesting antiferromagnetic interactions in these compounds, as corroborated by the negative Weiss temperatures. The magnetisation isotherms at 4 K (Figure 8) show almost linear behaviour that also confirms the preponderance of the antiferromagnetic interactions. However, the observed splitting of the ZFC and FC curves at low temperatures (Figures 6 and 7) indicates some kind of spin-glass like behaviour. The *ac* susceptibility measurements confirm this behaviour. Both parts of the susceptibility (the real and the imaginary part) present two peaks: the peak at higher temperatures is frequency independent and corresponds to the long-range antiferromagnetic ordering, whereas the second peak at lower temperatures is frequency dependent and approximately coincides with the onset of the ZFC-FC divergence in the *dc* curves. On increasing the frequency, the intensity of this maximum shifts to higher temperatures and this behaviour is characteristic of a spin-glass like state.[19]

A very common method for discerning if the material presents spin-glass behaviour is using the following equation:

$$K = \frac{\Delta T_g}{T_g \Delta \ln(f)}$$

where T_g is the maximum in the χ' curve, f is the frequency and Δ refers to differences between measurements at different frequencies.[20] For spin glasses, K is found to be of the order of 0.01, approximately in between 0.005 and 0.2. For $NdMn_{1.5}Ru_{0.5}O_5$, $K = 0.014$ which is consistent with the spin-glass category. The absence of long range magnetic ordering confirmed by low-temperature neutron diffraction is also compatible with the presence of a spin-glass state.

Although the random distribution of Ru^{4+} cations in the chains of $Mn^{4+}O_6$ octahedra should account for the existence of competitive magnetic interactions and a large degree of frustration in this compound, leading to the observed spin-glass behaviour, it is important to notice that in the magnetic structure of $NdMn_2O_5$ there already exists an important degree of magnetic frustration. In the parent compound, there are competitive interactions between the clearly antiferromagnetic coupling in Mn^{3+}(pyramids)–O–Mn^{4+}(chains), the latter tending to form ferromagnetic dimers of Mn^{4+} spins along the chains (as happens in $BiMn_2O_5$[21]) and the direct antiferromagnetic interactions established across the Mn^{4+}–O–Mn^{4+} paths along the chains, giving rise to an incommensurate helicoidal structure, modulated along the chain direction. The presence of Ru–Ru dimers randomly distributed along the chains of octahedra seems to reinforce the global magnetic interactions and reduce the frustration, leading to a significant increase of T_N (Table 5). Presumably the coupling between the two members of each Ru–Ru dimer is ferromagnetic, as suggested by the global increase of the Weiss temperature (that becomes less negative) upon Ru doping.

From this point of view, it is well known that some cubic perovskites containing Ru^{4+} cations show ferromagnetic behaviour, such as the paradigmatic examples of the cubic $BaRuO_3$ or $SrRuO_3$ perovskites.[22] On the other hand, hexagonal 6H-$BaRuO_3$, containing dimers of $Ru^{4+}O_6$ face-sharing octahedra separated by single RuO_6 corner sharing octahedra presents exchange-enhanced Pauli paramagnetism due to a strong electron correlation effect.[23] In 6H-$BaRu_{1-x}Mn_xO_3$ perovskites, the substitution of Mn for Ru cations gives rise to the short-range magnetic ordering, due to the disordered arrangement of Ru and Mn cations. The compounds are weakly ferromagnetic in the x range 0.05–0.40, with the maximal Curie temperature $T_C = 175.2$ K at $x = 0.10$. They show a spin-glass-like magnetism at lower temperature when $x \geq 0.1$.[24] Also, heavily substituted $SrMn_{1-x}Ru_xO_3$ materials are ferromagnetic due to dominating exchange interactions between the Ru^{4+} ions. Intermediate substitution ($0.6 \leq x \leq 0.7$) leads to spin-glass behaviour,[25] as observed in the present compound. The behaviour of other mixed Mn/Ru phases is also enlightening: the crystal and magnetic structures of the $(Nd_{1-x}Sr_x)(Mn_{1-x}Ru_x)O_3$ perovskites show an unusual long-range ferromag-

netic state which can be called "statistical ferrimagnetism" with antiferromagnetic coupling between Mn and Ru magnetic moments and ferromagnetic coupling in the Mn–Mn and Ru–Ru pairs.[26] This is not exactly our case, since the presence of the additional AFM couplings between the octahedral cations and Mn^{3+} in pyramidal positions can impose a global antiferromagnetic structure (as shown from the linear M vs. H curves in Figure 8) but it gives some clues about the probable coupling of the Ru dimers characterising the $NdMn_{1.5}Ru_{0.5}O_5$ oxide.

Conclusions

A new family of oxides has been obtained by replacing Mn^{4+} by Ru^{4+} in the parent $NdMn_2O_5$ compound. A NPD study confirms that these oxides are isostructural with the parent material (space group *Pbam*) and contain chains of edge-linked $(Mn,Ru)^{4+}O_6$ octahedra connected by means of dimeric groups of $Mn^{3+}O_5$ square pyramids. A unique feature of the $x = 0.5$ member is the occurrence of Ru–Ru metal–metal bonding within the chains of octahedra as has been frequently observed in many hexagonal ABO_3 polytypes of perovskite (e.g. $BaRuO_3$) where a metal–metal bonding is established though the triangular faces of the RuO_6 octahedra containing hexagonal stackings of face-sharing octahedra. $NdMn_{1.5}Ru_{0.5}O_5$ constitutes a unique case where the metal–metal bonding is established though edge-sharing octahedra. The Ru–Ru distances of 2.6026(4) Å are slightly longer than those observed in $BaRuO_3$. In $NdMn_{1.5}Ru_{0.5}O_5$, only half of the octahedral position are occupied by Ru and the absence of superstructure peaks in the XRD or NPD patterns indicates the absence of long-range ordering of Mn/Ru along the chains. We propose a structural model where pairs of Ru^{4+}–Ru^{4+} cations are randomly distributed along the chains together with Mn^{4+} cations, with no coherence between adjacent unit cells. The magnetic susceptibility plots show a divergence between the ZFC and FC curves, suggesting spin-glass behaviour which is confirmed by *ac* susceptibility measurements.

Experimental Section

Single-phase products of composition $NdMn_{2-x}Ru_xO_5$ ($0 < x \leq 0.5$) were obtained as very dark-brown polycrystalline powders from a citrate technique derived from that described elsewhere for the RMn_2O_5 oxides.[27] Stoichiometric amounts of analytical grade Nd_2O_3 and $MnCO_3$ were dissolved in an aqueous citric acid solution with some droplets of HNO_3 and then RuO_2 was added. The suspension was slowly evaporated leading to an organic resin which was dried at 140 °C and slowly decomposed at 600 °C in air. All the organic materials and nitrates were eliminated in a subsequent treatment at 800 °C in air. By this method very reactive precursors can be obtained. The precursor powders were then annealed at 1000 °C in air. It was not possible to synthesise single-phased materials with $x > 0.5$. In those cases we observed phase segregation of the RuO_2 and $NdMnO_3$ oxides. Trials to stabilise other isostructural compounds with rare earths other than Nd (Y, La, Tb, Dy, Ho, Er, Tm, Yb and Lu) were unsuccessful.

The reaction products ($0 < x \leq 0.5$) were characterised by X-ray diffraction (XRD) for phase identification and to asses phase purity. The characterisation was performed using a Bruker-axs D8 diffractometer (40 kV, 30 mA) in Bragg–Brentano reflection geometry with Cu-K_α radiation (λ = 1.5418 Å). The XRD patterns were analysed by the Rietveld method[28] by using the Fullprof program.[29]

Neutron powder diffraction (NPD) diagrams were collected for the $x = 0.5$ sample at the Institut Laue-Langevin, Grenoble (France). The diffraction patterns were acquired on the D1A diffractometer with λ = 1.910 Å at room temperature (295 K), in the angular range $10.0° < 2\theta < 150°$ with a 0.05° step and on the D1B diffractometer with λ = 2.520 Å at 2 K, in the angular range $10.0° < 2\theta < 80°$. The sample was contained in a vanadium cylinder, 8 mm in diameter. The NPD patterns were also analysed by the Rietveld method. A pseudo-Voigt function was considered to generate the profile shape and the background was fitted to a fifth-degree polynomial function. The coherent scattering lengths for Nd, Mn, Ru and O were 7.690, –3.730, 7.030 and 5.803 fm, respectively. An absorption correction $\mu r = 0.5$, estimated for the diameter of the sample cylinder, was introduced.

The *dc* magnetic susceptibility was measured with a SQUID magnetometer from Quantum Design equipped with a 70 kOe superconducting magnet, in the temperature interval $4 < T < 400$ K in a 1 kOe magnetic field. An isothermal magnetisation curve was obtained at 4 K for a magnetic field ranging from –50 to 50 kOe.

A PPMS device was used for carrying out *ac* magnetic susceptibility measurements for temperatures form 2 K to 100 K. The frequencies for the transversal oscillating magnetic field were 1, 2, 3, 4, 5, 6, 7, 8, 9 and 10 kHz.

Acknowledgments

We thank the financial support of Comisión Interministerial de Ciencia y Tecnología (CICyT) to the project MAT2007-60537 and to the project MAT2008-06517-C02-01. We are grateful to Institut Laue Langevin (ILL) of Grenoble for making all facilities available.

[1] K. Saito, K. Kohn, *J. Phys. Condens. Matter* **1995**, *7*, 2855–2863.
[2] A. Inomata, K. Kohn, *J. Phys. Condens. Matter* **1996**, *8*, 2673–2678.
[3] Y. F. Popov, A. M. Kadomtseva, S. S. Krotov, G. P. Vorob'ev, M. M. Lukina, *Ferroelectrics* **2002**, *279*, 147–156.
[4] Y. F. Popov, A. M. Kadomtseva, S. S. Krotov, G. P. Vorob'ev, K. I. Kamilov, M. M. Lukina, M. M. Tegranchi, *J. Exp. Theor. Phys.* **2003**, *96*, 961–965.
[5] V. A. Sanina, L. M. Sapozhnikov, E. I. Golovenchits, N. V. Morozov, *Sov. Phys. Solid State* **1988**, *30*, 1736–1740.
[6] E. I. Golovenchits, N. V. Morozov, V. A. Sanina, L. M. Sapozhnikova, *Sov. Phys. Solid State* **1992**, *34*, 56–59.
[7] K. Kohn, I. Kagomiya, *J. Cryst. Soc. Jpn.* **1999**, *41*, 342–346.
[8] S. Quezel-Ambrunaz, E. F. Bertaud, G. C. Buisson, *C. R. Acad. Sci.* **1964**, *258*, 3025–3028.
[9] E. F. Bertaud, G. C. Buisson, A. Durif, A. Mareschal, M. C. Montmory, S. Quezel-Ambrunaz, *Bull. Soc. Chim. Fr.* **1965**, 1132–1137.
[10] J. A. Alonso, M. T. Casais, M. J. Martínez-Lope, J. L. Martínez, M. T. Fernández-Díaz, *J. Phys. Condens. Matter* **1997**, *9*, 8515–8526.
[11] A. Muñoz, J. A. Alonso, M. J. Martínez-Lope, J. L. Martínez, *Chem. Mater.* **2004**, *16*, 4087–4090.
[12] A. Muñoz, J. A. Alonso, M. J. Martínez-Lope, J. L. Martínez, *Eur. J. Inorg. Chem.* **2007**, 1972–1979.

[13] A. Muñoz, J. A. Alonso, M. J. Martínez-Lope, J. L. Martínez, *Phys. Rev. B* **2005**, *72*, 184402-8.
[14] J. A. Alonso, M. J. Martínez-Lope, M. T. Casais, J. L. Martínez, V. Pomjakushin, *Eur. J. Inorg. Chem.* **2005**, 2600–2606.
[15] M. J. Martínez-Lope, M. Retuerto, J. A. Alonso, V. Pomjakushin, *J. Solid State Chem.* **2008**, *181*, 2155–2160.
[16] C. de la Calle, J. A. Alonso, M. J. Martínez-Lope, M. García-Hernández, G. André, *Mater. Res. Bull.* **2008**, *43*, 197–206.
[17] M. L. Foo, Q. Huang, J. W. Lynn, W.-L. Lee, T. Klimczuk, I. S. Hagemann, N. P. Ong, R. J. Cava, *J. Solid State Chem.* **2006**, *179*, 563–572.
[18] R. D. Shannon, *Acta Crystallogr., Sect. A* **1976**, *32*, 751–767.
[19] A. Durand, O. Mentre, F. Abraham, T. Fukuda, B. Elouadi, *Solid State Sci.* **2006**, *8*, 155–161.
[20] J. A. Mydosh, *Spin Glasses*, Taylor & Francis, London, **1993**.
[21] A. Muñoz, J. A. Alonso, M. T. Casais, M. J. Martínez-Lope, J. L. Martínez, M. T. Fernández-Díaz, *Phys. Rev. B* **2002**, *65*, 144423-8.
[22] J. S. Zhou, K. Matsubayashi, Y. Uwatoko, C. Q. Jin, J. G. Cheng, J. B. Goodenough, Q. Q. Liu, T. Katsura, A. Shatskiy, E. Ito, *Phys. Rev. Lett.* **2008**, *101*, 077206-4.
[23] J. G. Zhao, L. X. Yang, Y. Yu, F. Y. Li, R. C. Yu, Z. Fang, L. C. Chen, C. Q. Jin, *J. Solid State Chem.* **2007**, *180*, 2816–2823.
[24] J. G. Zhao, L. X. Yang, Y. Yu, F. Y. Li, R. C. Yu, C. Q. Jin, *J. Solid State Chem.* **2008**, *181*, 1767–1775.
[25] S. Kolesnik, B. Dabrowski, O. Chmaissem, *Phys. Rev. B* **2008**, *78*, 214425-7.
[26] A. M. Balagurov, S. N. Bushmeleva, V. Y. Pomjakushin, D. V. Sheptykov, V. A. Amelichev, O. Y. Gorbenko, A. R. Kaul, E. A. Gan'shina, N. B. Perkins, *Phys. Rev. B* **2004**, *70*, 014427-8.
[27] J. A. Alonso, M. J. Martínez-Lope, M. T. Casais, J. L. Martínez, I. Rasines, *J. Solid State Chem.* **1997**, *129*, 105–112.
[28] H. M. Rietveld, *J. Appl. Crystallogr.* **1969**, *2*, 65–71.
[29] J. Rodriguez-Carvajal, *Phys. B* **1993**, *192*, 55–69.

Received: July 2, 2009
Published Online: January 4, 2010

